Toward Ultrahigh Red Light Responsive Organic FETs Utilizing Neodymium Phthalocyanine as Light Sensitive Material

Lei Sun, Yao Li, Qiang Ren, Wenli Lv, Jianping Zhang, Xiao Luo, Feiyu Zhao, Zhen Chen, Zhanwei Wen, Junkang Zhong, Yingquan Peng, and Xingyuan Liu

***Abstract*— The performance of photoresponsive organic FETs (photOFETs) intimately depends on their optical absorption and charge carrier transport property. We report on red light responsive photOFETs based on various device structures utilizing neodymium phthalocyanine ($NdPc_2$) as the light sensitive material. PhotOFETs based on planar heterojunction, bulk heterojunction (BHJ), and hybrid planar–BHJ (HPBHJ) with $NdPc_2$ and C_{60} on poly(vinyl alcohol) (PVA) and SiO_2 gate dielectric were fabricated and characterized. Among various device structures, HPBHJ-photOFET on PVA dielectric showed the best performance. For the 650-nm-red light illumination, an ultrahigh photoresponsivity of 108 A/W and a maximum photosensitivity of 3.75×10^4 were obtained. The ultrahigh enhancement of the photoresponsivity for HPBHJ-photOFET is resulted from high absorption coefficient of $NdPc_2$ in the red light region, high dissociation efficiency of the photogenerated excitons, and high electron mobility of C_{60} layer grown on PVA.**

***Index Terms*— Gate dielectric, hybrid bulk–planar heterojunction, neodymium phthalocyanine ($NdPc_2$), photoresponsive organic FET (photOFET), photoresponsivity, poly(vinyl alcohol) (PVA), red light.**

I. Introduction

ORGANIC FETs (OFETs) are envisaged to be pervasive in the future generation electronic products that have some unconventional characteristics, such as low cost, light weight, mechanical flexibility, and large-area coverage [1]–[3]. Among OFETs, the photoresponsive OFET (photOFET), as an important component of photodetectors, has aroused researchers' enormous interests in recent years [4]–[6]. Compared with photodiodes, photOFETs exhibit lower noise and higher light sensitivity [7]. The performance of photOFETs intimately depends on the properties of organic photoelectric functional materials, i.e., the coefficient for light absorption and the mobility for charge carrier transport. For traditional single layer photOFETs, light absorption and photocarrier transport are accomplished in a single organic layer, which severely limits the device performance due to the fact that the charge carrier mobility of most photosensitive organic thin films is very low. Therefore, organic heterostructure becomes an ideal strategy for realizing high-performance photoelectron devices, which has been widely exploited in organic light-emitting diodes [8]–[10], OFETs [11], [12], and organic solar cells (OSCs) [13]–[16]. In particular, a hybrid planar–bulk heterojunction (HPBHJ) structure is favored, which is composed of a high mobility channel transport layer (CTL) and a photosensitive layer with highly efficient exciton dissociation efficiency that uses a donor–acceptor (DA) BHJ structure [17]. Neodymium phthalocyanine ($NdPc_2$), as one of the rare earth phthalocyanines, shows an outstanding red light absorption characteristic [18], [19] and an excellent semiconductor property, which can be used as the photosensitive material in red light detectors. In addition, fullerene (C_{60}), being a good electron acceptor with a high electron mobility of 4.9 cm^2/Vs [20], is extensively applied in OFETs [21], [22] and OSCs [23]–[25]. Recently, we reported on a photOFET with a novel structure of HPBHJ, which demonstrated superior performance compared with that with a BHJ structure or a planar heterojunction (PHJ) structure [17]. Here, we fabricated an ultrahigh red light responsive HPBHJ-photOFET utilizing $NdPc_2$ as light absorption material and C_{60} grown on poly(vinyl alcohol) (PVA) as the CTL, which exhibited an ultrahigh red light responsibility of 108 A/W and photosensitivity of 3.75×10^4, which are exceed or comparable with the record values reported in [26]–[28].

II. Experimental Detail

PVA (99% purity, low molecular weight) was purchased from Alfa Aesar and C_{60} (99.5% purity) from Lum. Tech. Ltd.,

Manuscript received August 23, 2013; revised October 29, 2015; accepted October 29, 2015. Date of publication November 23, 2015; date of current version December 24, 2015. This work was supported in part by the National Natural Science Foundation of China under Grant 10974074 and in part by the Research Fund for the Doctoral Program of Higher Education of China under Grant 20110211110005. The review of this paper was arranged by Editor D. J. Gundlach.

L. Sun, Y. Li, Q. Ren, W. Lv, J. Zhang, X. Luo, F. Zhao, Z. Wen, and J. Zhong are with the School of Physical Science and Technology, Institute of Microelectronics, Lanzhou University, Lanzhou 730000, China (e-mail: sunl12@lzu.edu.cn; l_y_2010@lzu.edu.cn; renq14@lzu.edu.cn; lvwl10@lzu.edu.cn; zhangjp13@lzu.edu.cn; luox12@lzu.edu.cn; 1005792402@qq.com; 1209027776@qq.com; zhongjk13@lzu.edu.cn).

Z. Chen is with the College of Optical and Electronic Technology, China Jiliang University, Hangzhou 310018, China (e-mail: sgn91.8@gmail.com).

Y. Peng is with the School of Physical Science and Technology, Institute of Microelectronics, Lanzhou University, Lanzhou 730000, China, and also with the College of Optical and Electronic Technology, China Jiliang University, Hangzhou 310018, China (e-mail: yqpeng@lzu.edu.cn).

X. Liu is with the Changchun Institute of Optics, Fine Mechanics and Physics, Chinese Academy of Sciences, Changchun 130024, China (e-mail: liuxy@ciomp.ac.cn).

Color versions of one or more of the figures in this paper are available online at http://ieeexplore.ieee.org.

Digital Object Identifier 10.1109/TED.2015.2497353

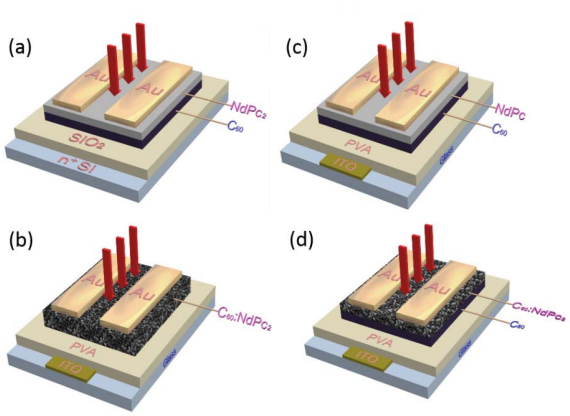

Fig. 1. Schematic of the device structure for (a) Device A, (b) Device B, (c) Device C, and (d) Device D.

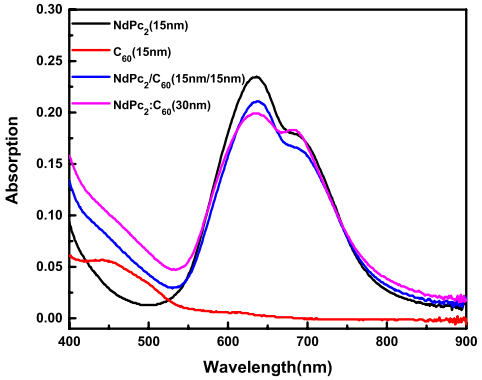

Fig. 2. Optical absorption spectrum of thin films of C_{60} (15 nm), $NdPc_2$ (15 nm), $C_{60}/NdPc_2$ (15/15 nm), and $NdPc_2$:C_{60} (30-nm weight ratio 1:1) on the quartz glasses.

both of which were used as received. $NdPc_2$ was synthesized according to the method reported in [29] and purified by vacuum sublimation before use. As shown in Fig. 1, five kinds of photOFETs with the bottom-gate top-contact structure were fabricated on either SiO_2 dielectric or PVA dielectric. Device A is in the structure of n^+-Si/SiO_2/C_{60}/$NdPc_2$/Au(S&D) with the PHJ structure [Fig. 1(a)], Device B is in the structure of ITO/ PVA/C_{60}:$NdPc_2$/Au(S&D) with the BHJ structure [Fig. 1(c)], Device C is ITO/PVA/C_{60}/$NdPc_2$/Au(S&D) with the PHJ structure [Fig. 1(b)], and Device D is ITO/PVA/C_{60}/C_{60}:$NdPc_2$/Au(S&D) with the HPBHJ structure [Fig. 1(d)]. For comparison, Device E ITO/PVA/C_{60}/Au(S&D) was also fabricated. Herein, S&D denotes source and drain electrodes.

For fabrication of Device A, a heavily n-doped Si substrate with a resistivity of 0.03 $\Omega \cdot$cm acts as the gate electrode and substrate, and a thermally grown SiO_2 layer as the gate dielectric for SiO_2-based photOFETs. The SiO_2 substrates were ultrasonically cleaned by acetone, ethanol, and deionized water, and were dried with N_2 gas blowing and baked in an oven with a temperature of 60 °C for 20 min. Then, a 50-nm-thick C_{60} film and a 15-nm $NdPc_2$ film were sequencially deposited on the top of either SiO_2 at the rate of 0.01 and 0.015 nm/s, respectively, at room temperature. Au source–drain electrodes were thermally evaporated at the rate of 0.095 nm/s through a shadow mask to define a channel with a length (L)/a width (W) of 50 μm/2 mm.

For the fabrication of PVA dielectric-based photOFETs, ITO glass substrates were coated with a tape partly and, then, etched in HCl solutions (20 min) to form strip patterned gate (5 mm × 30 mm) at room temperature, and then, were rinsed with acetone, ethanol, and deionized water in an ultrasonic bath, dried by blowing high-pure N_2 gas and baked in an oven at 60 °C. Subsequently, PVA solution (20% in water) was spun at 3000 r/min on the top of ITO substrates to form around 1100-nm-thick PVA film with a capacitance per unit area of 4.24 nF/cm^2, and then the films were dried in a vacuum oven at 80 °C for 2 h. To improve the property of PVA dielectric, the PVA thin film on ITO substrates were cross-linked at 200 °C for 2 h in a vacuum oven. For the photOFET fabrication, at first, a 50-nm-thick C_{60} film was vacuum deposited on the top of PVA at the same rate of 0.01 nm/s; then, a 15-nm-thick $NdPc_2$ film (Device B) or a 30-nm-thick $NdPc_2$:C_{60} (weight ratio 1:1, Device C) film were vacuum deposited on the top of C_{60} film at the rate of 0.01 nm/s. For comparison, a 50-nm-thick C_{60} film (Device E) was directly deposited on the top of PVA (Device E) at the same rate of 0.01 nm/s. The vacuum during deposition was kept at 2.0×10^{-3} Pa. Au source–drain electrodes were fabricated as the same of Device A. The electrical characteristics of devices were measured under the same conditions as the previous experiment [34]. Top illumination was performed using a red laser diode with a central wavelength of 650 nm, and neutral density filters were used to adjust the light intensity. The absorption spectra of the thin films on cleaned quartz substrates were measured by the TU-1901 spectrometer. All measurements were performed at room temperature.

III. Results and Discussion

As shown in Fig. 2, C_{60} film (15 nm) has no obvious absorption in the red light region (620–770 nm), and the absorption spectra of $NdPc_2$ (15 nm), $C_{60}/NdPc_2$ (50/15 nm), and C_{60}:$NdPc_2$ (30 nm) films are overlapped in the red region. Owing to wideband gap (2.6 eV) of C_{60} [30], its optical absorption is mainly in the UV region, and thus, the optical absorption of $C_{60}/NdPc_2$ and C_{60}:$NdPc_2$ films in the red region mainly originates from $NdPc_2$. In addition, the maximum absorption coefficient at Q-band of $NdPc_2$ film deposited on a quartz substrate can reach up to 1.7×10^5 cm^{-1} [31], which is greater than that of CuPc (valued 5.6×10^4 cm^{-1}), PbPc (valued 1.1×10^5 cm^{-1}) [17], PdPc (valued 1.0×10^5 cm^{-1}) [32], and pentacene (valued 5.2×10^4 cm^{-1}) [33]. Thus, NdPc is a competitive candidate as a light-sensitive material for red light detector.

A. PHJ-photOFET on SiO_2 Dielectric

Device A exhibits typical n-channel FET characteristics [Fig. 3(a) and (b)]. From Table I, we can see that at $V_d = 50$ V and $V_g = 100$ V, the photoresponsivity (R) and the maximum ratio of photocurrent to dark current ($P_{\max}$) of Device A are 806 mA/W and 335 under an illumination

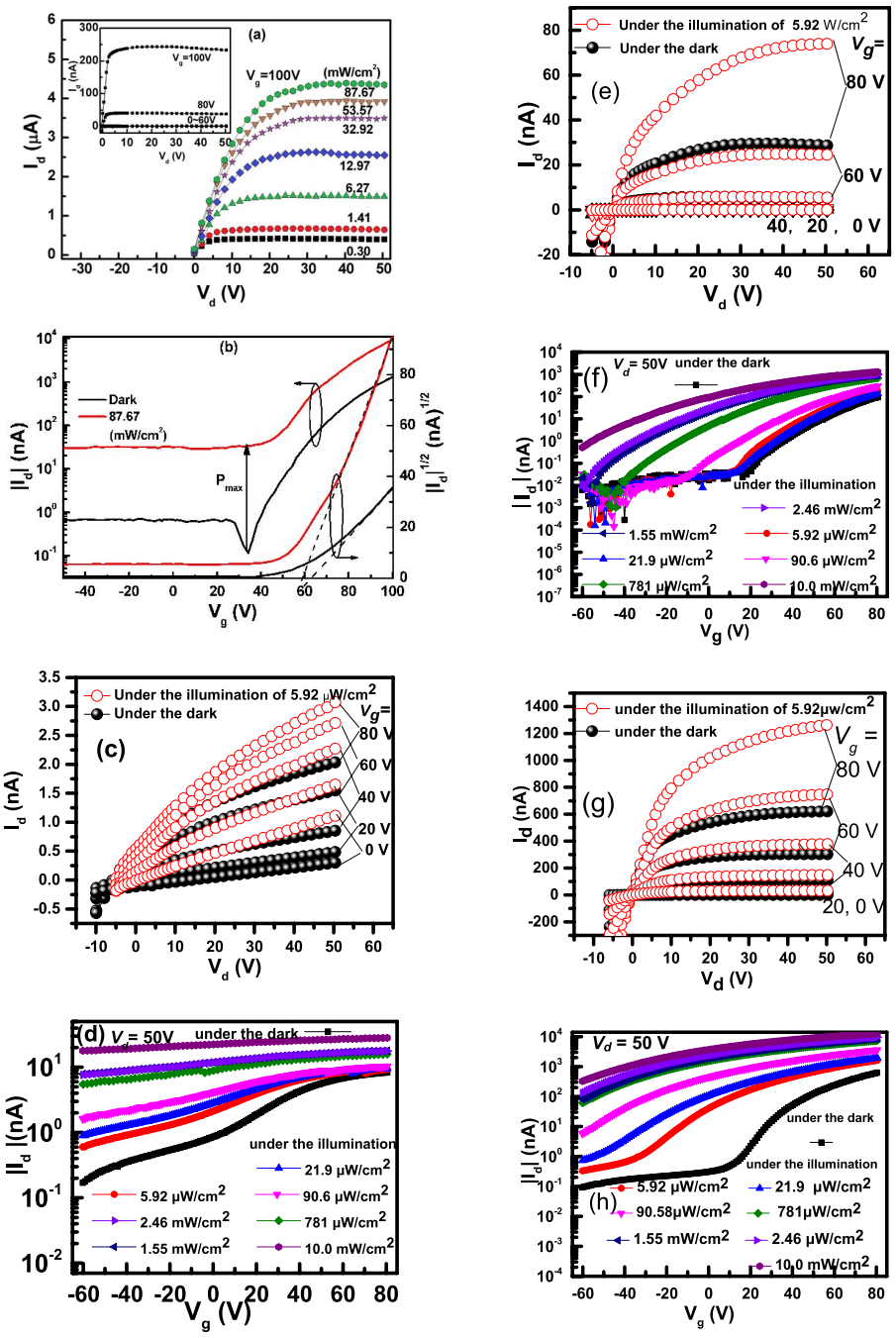

Fig. 3. Output and transfer characteristics of Device A (PHJ-photOFET on SiO_2 dielectric): (a) and (b), the inset is under the dark; Device B (PHJ-photOFET on PVA dielectric): (c) and (d); Device C (PHJ-photOFET on PVA dielectric): (e) and (f) Device D (HPBHJ- photOFET on PVA dielectric): (g) and (h).

intensity of 87.67 mW/cm^2, respectively. Actually, both the responsivity and the photocurrent to dark current ratio are much less than those of Device C that is manufactured on PVA dielectric.

B. BHJ-photOFET on PVA Dielectric

The output and transfer characteristics of Device B are shown in Fig. 3(c) and (d), from which n-channel FET characteristics were observed. In the dark, the drain current (I_d) of Device A at drain voltage $V_d = 50$ V and gate voltage $V_g = 80$ V was 2.03 nA, while under the illumination, the I_d value of Device A increased by a factor of 1.51–3.07 nA. It can be seen from Fig. 3(d) that with increasing incident light intensity, the I_d value of Device B increases. Upon illumination, $NdPc_2$ film absorbs photons to generate excitons, a part of which reached the $NdPc_2/C_{60}$ interface and are dissociated there to become free holes and electrons. The free holes transport to the source electrode and the free electrons to the drain electrode under the influence of the electric field, respectively.

TABLE I

DEVICE PERFORMANCE DETAILS AT $V_d = 50$ V. VALUES OF SATURATION MOBILITY AND THRESHOLD VOLTAGE WERE EXTRACTED FROM THE TRANSFER CURVES BY USING (2) AND EXPERIMENTAL DATA

Device	Structure	$I_{d,\text{dark}}$ (nA)	$I_{d,\text{ill}}$ (nA)	R (A/W)	P_{max}	$\mu_{\text{sat, dark}}$ (cm^2/Vs)	$\mu_{\text{sat, ill}}$ [b] (cm^2/Vs)	$V_{th,\text{dark}}$ (V)	$V_{th,\text{ill}}$, [d] (V)	EQE (%)
Device A	Si/SiO_2/ C_{60}/$NdPc_2$/Au(S&D)	30	496	0.800[a]	1.65×10^{2} [c]	7.4×10^{-3}	2.88×10^{-2} [a]	64	60 [a]	152.70
Device B	ITO/PVA/ C60:$NdPc_2$ /Au (S&D)	2.03	3.07	0.175[b]	0.175[b]	1.37×10^{-5}	9.12×10^{-6} [b]	-20.3	-51.1 [b]	33.40
Device C	ITO/PVA/C_{60}/$NdPc_2$/Au(S&D)	28	78	7.64[b]	3.31×10^{4} [d]	9.75×10^{-4}	1.35×10^{-3} [b]	50.9	41.6 [b]	1458
Device D	ITO/PVA/C_{60}/C_{60}:$NdPc_2$/Au(S&D)	782	1293	108[b]	3.75×10^{4} [d]	2.64×10^{-3}	2.65×10^{-3} [b]	27.6	-4.04 [b]	20612

[a] The result was obtained under the illumination of 1.41mW/cm^2.
[b] The result was obtained under the illumination of 5.92μW/cm^2.
[c] The result was obtained at Vg= 34V under the illumination of 87.67mW/cm^2.
[d] The result was obtained at Vg=-60V,-40V and 1V for Device B,C,D respectively under the illumination of 10.0mW/cm^2 .

An important parameter for photOFETs is the photoresponsivity, R, which is defined as the ratio of photocurrent I_{ph} to the incident optical power P_{opt}, that is, $R = I_{\text{ph}}/P_{\text{opt}} = I_{\text{ph}}/(\text{AP}_{\text{int}})$, where A is the channel area and P_{int} is the optical intensity. From the photoresponsivity, the external quantum efficiency (EQE) can be expressed by [17]

$$\text{EQE} = \frac{hc}{q\lambda}R. \tag{1}$$

Here, h, c, and q are the Planck constant, the velocity of light in vacuum, and the elementary electric charge, respectively; λ is the wavelength of incident light. Another important parameter for photOFETs is photosensitivity P, which is defined as the ratio of photocurrent I_{ph} to the dark drain current $I_{d,\text{dark}}$, that is, $P = I_{\text{ph}}/I_{d,\text{dark}}$. At $V_d = 50$ V and $V_g = 80$ V, an R of 0.175 A/W was achieved under the 5.92-μW/cm^2 illumination. From (1), an EQE of 33.40% was calculated. Under the 10-mW/cm^2 illumination, a maximum photosensitivity P_{max} of 1.14×10^2 was achieved at $V_d = 50$ V and $V_g = -60$ V.

The charge transport ability of OFETs can be characterized by the saturation region mobility (μ_{sat}), which can be extracted from

$$I_d = \frac{1}{2}\mu_{\text{sat}}C_i\frac{W}{L}(V_g - V_{\text{th}})^2 \quad V_d > (V_g - V_{\text{th}}). \tag{2}$$

Here, V_{th} is the threshold voltage, W and L are the channel width and length, respectively, and C_i is the capacitance per unit area of gate dielectric. The μ_{sat} of Device C was calculated to be 2.64×10^{-3} cm^2/Vs.

C. PHJ-photOFET on PVA Dielectric

The output and transfer characteristics of Device C (PHJ structure) are shown in Fig. 3(e) and (f). Similar to Device B, the typical n-type FET characteristics are observed. Both the dark current ($I_{d,\text{dark}}$) and the photocurrent (I_{ph}) of Device C are larger than those of Device B. The $I_{d,\text{dark}}$ value of Device C at $V_d = 50$ V and $V_g = 80$ V was 33.3 nA, which is 16.3 times larger than that of Device B [2.03 nA, Fig. 3(a)]. As listed in Table I, at $V_d = 50$ V and $V_g = 80$ V, the R value of Device C is 7.64 A/W under the 5.92-μW/cm^2 illumination, and P_{max} is 3.31×10^4 under the 10- mW/cm^2 illumination, which are 43.7 times and 290 times larger than those of Device B, respectively. From (1), an EQE of 1488% was calculated for Device C. The physical process occurring in Device C

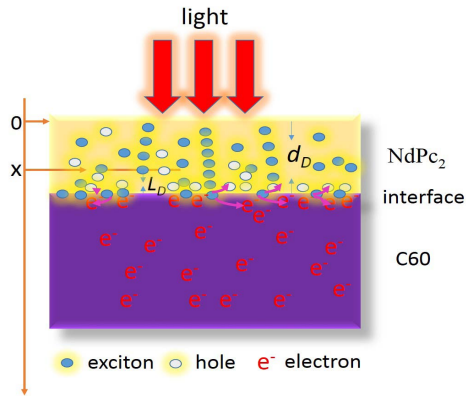

Fig. 4. Schematic of exciton diffusion in a PHJ by light illumination.

under the illumination can be described as follows [17]: when illuminated, the $NdPc_2$ photosensitive layer absorbs incident photons to generate excitons, and a part of which diffuse to $NdPc_2$/C_{60} interface and dissociate into free holes in $NdPc_2$ layer and free electrons in C_{60} layer. Under the influence of the electric field, the free electrons move in C_{60} layer, cross the C_{60}/$NdPc_2$ interface into $NdPc_2$ layer, and finally, reach the drain electrode, while the free holes move to source electrode. Compared with BHJ photOFETs, PHJ photOFETs exhibit higher channel mobility, but lower exciton dissociation efficiency. We consider that the better performance of Device C (PHJ-photOFET) than Device B (BHJ-photOFET) may be the result that the positive effect of high mobility of CTL overwhelms the negative effect of low exciton diffusion efficiency of PHJ in Device C.

Assuming that Lambert–Beer's law holds for light absorption in the organic film, and let I_0 be the incident light intensity, then the light intensity at position x in the NdPc film (Fig. 4) can be expressed by the following equation:

$$I = I_\circ e^{-\alpha x}. \tag{3}$$

Here, α is the absorption coefficient. Under the illumination, the excitons were photogenerated in the $NdPc_2$ layer. Then, the excitons diffused to the DA interface, i.e., $NdPc_2$/C_{60} interface as schematically shown in Fig. 4. In Fig. 4, d_D is the thickness of $NdPc_2$ layer, and L_D is the diffusion length of the exciton. Under the light illumination, the number of photons absorbed in $NdPc_2$ is $(I_\circ - I_\circ e^{-\alpha d_D})/h\nu$, where $h\nu$ is photo energy. If one absorbed photon can generate one exciton,

then the number of excitons that can reach the DA interface by diffusion is $0.5(I_\circ e^{-\alpha(d_D-L_D)} - I_\circ e^{-\alpha d_D})/h\nu$. In general, the photogenerated excitons will diffuse in all directions. Here, we assume that the excitons diffuse only in the up and down direction due to the thin $NdPc_2$ layer of only 15 nm. Then, the exciton diffusion efficiency η can be obtained

$$\eta = \frac{(I_\circ e^{-\alpha(d_D-L_D)} - I_\circ e^{-\alpha L_D})/h\nu}{2I_\circ(e^{\alpha d_D}-1)/h\nu} = \frac{e^{\alpha L_D}-1}{2(e^{\alpha d_D}-1)}. \quad (4)$$

Organic semiconductors with high charge carrier mobility have, in general, large exciton diffusion lengths. The hole mobility and exciton diffusion length of CuPc were reported to be 1.59×10^{-3} cm^2/Vs [35] and 8 nm [36], respectively. As the hole mobility of $NdPc_2$ is 7.5×10^{-5} cm^2/Vs [31], which is around one order of magnitude smaller than that of CuPc, we speculate that the exciton diffusion length of $NdPc_2$ should be less than that of CuPc, that is, less than 8 nm. With $L_D < 8$ nm, a diffusion efficiency of less than 25% is calculated for our PHJ device (Device C). This value should be much smaller than that of BHJ devices like Device B, which is usually up to 80%–90%, even 100% [37]–[39]. Therefore, the reason that the performance of the PHJ device is better than that of the BHJ device is due to the fact that the positive effect of high mobility of CTL overwhelms the negative effect of low exciton diffusion efficiency in PHJ devices like Device C.

D. HPBHJ- photOFET on PVA Dielectric

As shown in Fig. 3(g) and (h), the device exhibits typical n-channel FET characteristics. For a given drain voltage and gate voltage, the $I_{d,\text{dark}}$ and $I_{d,\text{ill}}$ values of Device D are larger than those of Device B or C, respectively. For example, the $I_{d,\text{dark}}$ value of Device D at $V_d = 50$ V and $V_g = 80$ V is 620 nA, which is 18.6 times larger than that of Device C (33.3 nA, Fig. 3) and 305 times larger than that of Device B (2.03 nA, Fig. 3), respectively. In fact, the μ_{sat} value of Device D is determined to be 2.64×10^{-3} cm^2/Vs, which is indeed 2.71 times larger than that of Device C.

As listed in Table I, the R value of Device D is as high as 108 A/W at $V_d = 50$ V and $V_g = 80$ V under the 5.92-$\mu W/cm^2$ illumination, which is 14.1 times larger than that of Device C. Under the 10-mW/cm^2 illumination, a $P_{\max}$ of 3.75×10^4 was achieved at $V_d = 50$ V and $V_g = 1$ V, which is comparable with that of Device C. This higher photoresponsivity of Device D in comparison with Device C originates from the higher exciton dissociation efficiency of $NdPc:C_{60}$ BHJ than that of $NdPc/C_{60}$ PHJ. From (1), an EQE of 20612% was calculated for Device D, which is much larger than those of Device B and Device C. Meanwhile, the EQE of Device C and Device D being greater than 100% under the illumination indicates that the photomultiplication effectively takes place as a result of conceivable charge trapping effect and a photoinduced drop of injection barrier [40]–[42].

In past years, Noh *et al.* [26] reported a red light (650 nm) responsivity of 0.15–0.45 A/W for pentacene photOFET. Afterward, Noh and Kim [27] reported a high red light responsivity of 1 A/W for pentacene photOFET. After that, Zhang *et al.* [28] reported a red light responsivity of 266.2 mA/W for a vertical structure photOFET based on copper phthalocyanine. Here, the R value of our fabricated HPBHJ photOFET reached a high value of 108 A/W, which is several orders of magnitude higher than that reported in the most publications and much larger than that of S1223-01 Si photodiodes (0.45 A/W, Hamamatsu Photonics K. K.), and is close to the record value of [33].

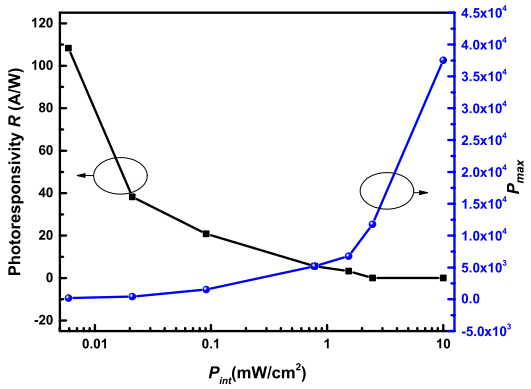

Fig. 5. Plots of photoresponsivity (R) and maximum photosensitivity ($P_{\max}$) versus incident optical intensity (P_{int}) for Device D.

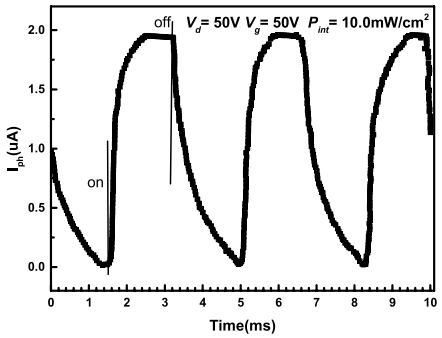

Fig. 6. Time response of Device D to the light pulses of the 650-nm wavelength and the 10-mW/cm^2 illumination.

The physical process occurring in an HPBHJ photOFET can be described as follows [17]: upon illumination, $NdPc_2$ molecules in C_{60}:$NdPc_2$ layer absorb incident photons to generate excitons, which dissociate into free holes and electrons with nearly 100% efficiency. Under the influence of the electric field, the free holes move to the source electrode contacting with the BHJ layer, while the free electrons first cross the BHJ/C_{60} interface and enter C_{60} channel layer, and then transport along the channel and reach the drain electrode. Fig. 5 shows the dependence of R and P on P_{opt} of Device C. The P value of Device C increases with P_{int}, while the value of R decreases with P_{int}.

The time response of Device D was also measured under the 5.92-$\mu W/cm^2$ illumination at $V_d = 50$ V and $V_g = 50$ V. A square-wave light signal is provided by the red laser diode of 650 nm and a light chopper with a frequency of 224 Hz. From Fig. 6, we can see that when the diode is turned ON, the current sharply increases to a certain value and keeps stable until the light is turned OFF. The rise time (from 10% to 90% of the maximum) and fall time (from 90% to 10% of the maximum) were approximately 0.6 and 1.8 ms, respectively.

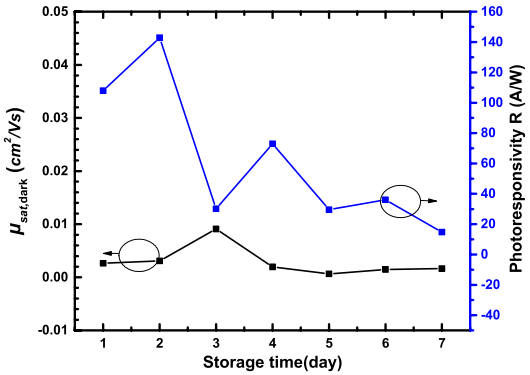

Fig. 7. Dependences of R under the illumination of 5.92 μW/cm^2 and $\mu_{\text{sat,dark}}$ on the storage time of Device D (HPBHJ-photOFET on PVA dielectric).

To characterize the long term stability, the dependences of device performances on the time of storage of the device in a rough vacuum (∼100 Pa) were measured. Fig. 7 shows the dependences of R and $\mu_{\text{sat,dark}}$ on the storage time. R decayed with the storage time, which exhibited a storage lifetime of 4.5 days (the storage time after which the photoresponsivity decays to the half of the initial value).

The decay of $\mu_{\text{sat,dark}}$ with storage time is much weaker than that of R and a storage lifetime larger than 7 days was obtained.

IV. Conclusion

In conclusion, PhotOFETs based on PHJ, BHJ, and HPBHJ composed of $NdPc_2$ and C_{60} on PVA and SiO_2 gate dielectric were fabricated and characterized. Among various device structures, HPBHJ-photOFET on PVA dielectric showed the best performance. For the 650-nm red light illumination of 5.92 μW/cm^2, an ultrahigh photoresponsivity of 108 A/W was obtained at $V_g = 80$ V and $V_d = 50$ V. For the light illumination of 10- mW/cm^2, a maximum photosensitivity of 3.75×10^4 was achieved at $V_d = 50$ V and $V_g = 1$ V. The achieved ultrahigh responsivity not only surpasses that of the commercial Si photodiodes, but also is several times larger than that of photOFETs reported in most literatures. The ultrahigh enhancement of photoresponsivity is resulted from the high absorption coefficient of $NdPc_2$ in the red light region, the high dissociation efficiency of the photo generated excitons in $NdPc_2$:C_{60} BHJ, and the high electron mobility of C_{60} film grown on PVA.

References

[1] B. Crone *et al.*, "Large-scale complementary integrated circuits based on organic transistors," *Nature*, vol. 403, pp. 521–523, Feb. 2000.

[2] H. Sirringhaus *et al.*, "High-resolution inkjet printing of all-polymer transistor circuits," *Science*, vol. 290, no. 5499, pp. 2123–2126, Dec. 2000.

[3] M. Halik and A. Hirsch, "The potential of molecular self-assembled monolayers in organic electronic devices," *Adv. Mater.*, vol. 23, nos. 22–23, pp. 2689–2695, Jun. 2011.

[4] B. Lucas, T. Trigaud, and C. Videlot-Ackermann, "Organic transistors and phototransistors based on small molecules," *Polym. Int.*, vol. 61, no. 3, pp. 374–389, Mar. 2012.

[5] K.-J. Baeg, M. Binda, D. Natali, M. Caironi, and Y.-Y. Noh, "Organic light detectors: Photodiodes and phototransistors," *Adv. Mater.*, vol. 25, no. 31, pp. 4267–4295, Aug. 2013.

[6] Y. Guo, G. Yu, and Y. Liu, "Functional organic field-effect transistors," *Adv. Mater.*, vol. 22, no. 40, pp. 4427–4447, Sep. 2010.

[7] T. P. I. Saragi, R. Pudzich, T. Fuhrmann, and J. Salbeck, "Organic phototransistor based on intramolecular charge transfer in a bifunctional spiro compound," *Appl. Phys. Lett.*, vol. 84, no. 13, p. 2334, Feb. 2004.

[8] A. Osinsky *et al.*, "MgZnO/AlGaN heterostructure light-emitting diodes," *Appl. Phys. Lett.*, vol. 85, no. 19, p. 4272, Sep. 2004.

[9] D. Qin, M. Wang, Y. Chen, L. Chen, and G. Li, "Electron injection via doped p–n heterojunction for inverted organic light emitting diodes," *Phys. Scripta*, vol. 89, no. 1, p. 015802, Feb. 2014.

[10] L. Deng *et al.*, "Pure and stable top-emitting white organic light-emitting diodes utilizing heterojunction blue emission layers and wide-angle interference," *ACS Appl. Mater. Interfaces*, vol. 6, no. 7, pp. 5273–5280, Mar. 2014.

[11] C. Rost, S. Karg, W. Riess, M. A. Loi, M. Murgia, and M. Muccini, "Light-emitting ambipolar organic heterostructure field-effect transistor," *Synth. Met.*, vol. 146, no. 3, pp. 237–241, Nov. 2004.

[12] C. Liu *et al.*, "Improving solution-processed *n*-type organic field-effect transistors by transfer-printed metal/semiconductor and semiconductor/semiconductor heterojunctions," *Organic Electron.*, vol. 15, no. 8, pp. 1884–1889, Aug. 2014.

[13] T. Nagata *et al.*, "Photoelectron spectroscopic study of band alignment of polymer/ZnO photovoltaic device structure," *Appl. Phys. Lett.*, vol. 102, no. 4, p. 043302, Jan. 2013.

[14] T. Yasuda, "Triphenylamine-based amorphous polymers for bulk-heterojunction photovoltaic cells," in *Proc. IOP Conf. Ser., Mater. Sci. Eng.*, vol. 54. May 2014, p. 012015.

[15] W. Ge, R. D. McCormick, G. Nyikayaramba, and A. D. Stiff-Roberts, "Bulk heterojunction PCPDTBT:PC_{71}BM organic solar cells deposited by emulsion-based, resonant infrared matrix-assisted pulsed laser evaporation," *Appl. Phys. Lett.*, vol. 104, no. 22, p. 223901, Jun. 2014.

[16] R. Shivanna *et al.*, "Charge generation and transport in efficient organic bulk heterojunction solar cells with a perylene acceptor," *Energy Environ. Sci.*, vol. 7, no. 1, pp. 435–441, Oct. 2014.

[17] Y. Peng *et al.*, "High performance near infrared photosensitive organic field-effect transistors realized by an organic hybrid planar-bulk heterojunction," *Organic Electron.*, vol. 14, no. 4, pp. 1045–1051, Apr. 2013.

[18] M. Moussavi, A. De Cian, J. Fischer, and R. Weiss, "(Porphyrinato)bis(phthalocyaninato)dilanthanide(III) complexes presenting a sandwich triple-decker-like structure," *Inorganic Chem.*, vol. 25, no. 13, pp. 2107–2108, Jan. 1986.

[19] N. E. Galanin and G. P. Shaposhnikov, "Sandwich complexes of yttrium, neodymium, gadolinium, and dysprosium with *meso-trans*-di(hexadecyl)-tetrabenzoporphyrin and phthalocyanine fragments. Synthesis and spectral properties," *Russ. J. Gen. Chem.*, vol. 82, no. 4, pp. 764–769, Jan. 2012.

[20] A. Virkar *et al.*, "The role of OTS density on pentacene and C_{60} nucleation, thin film growth, and transistor performance," *Adv. Funct. Mater.*, vol. 19, no. 12, pp. 1962–1970, Jun. 2009.

[21] R. Ahmed, A. Kadashchuk, C. Simbrunner, G. Schwabegger, M. A. Baig, and H. Sitter, "Geometrical structure and interface dependence of bias stress induced threshold voltage shift in C_{60}-based OFETs," *ACS Appl. Mater. Interfaces*, vol. 6, no. 17, pp. 15148–15153, Aug. 2014.

[22] W. Wang, J. Ying, J. Han, and W. Xie, "High mobility pentacene/C_{60}-based ambipolar OTFTs by thickness optimization of bottom pentacene layer," *IEEE Trans. Electron Devices*, vol. 61, no. 11, pp. 3845–3851, Nov. 2014.

[23] C.-F. Lin *et al.*, "Chloroboron subphthalocyanine/C_{60} planar heterojunction organic solar cell with N,N-dicarbazolyl-3,5-benzene blocking layer," *Solar Energy Mater. Solar Cells*, vol. 122, pp. 264–270, Mar. 2014.

[24] W. Chen, T. Salim, H. Fan, L. James, Y. M. Lam, and Q. Zhang, "Quinoxaline-functionalized C_{60} derivatives as electron acceptors in organic solar cells," *RSC Adv.*, vol. 4, no. 48, pp. 25291–25301, May 2014.

[25] T. Miyadera, Z. Wang, T. Yamanari, K. Matsubara, and Y. Yoshida, "Efficiency limit analysis of organic solar cells: Model simulation based on vanadyl phthalocyanine/C_{60} planar junction cell," *Jpn. J. Appl. Phys.*, vol. 53, no. 1S, p. 01AB12, Nov. 2014.

[26] Y.-Y. Noh, D.-Y. Kim, and K. Yase, "Highly sensitive thin-film organic phototransistors: Effect of wavelength of light source on device performance," *J. Appl. Phys.*, vol. 98, no. 7, p. 074505, Oct. 2005.

[27] Y.-Y. Noh and D.-Y. Kim, "Organic phototransistor based on pentacene as an efficient red light sensor," *Solid-State Electron.*, vol. 51, no. 7, pp. 1052–1055, Jul. 2007.
[28] Y. S. Zhang, M. Zhu, D. X. Wang, Z. Y. Wang, Y. Y. Wang, and J. H. Yin, "The fabrication and characteristics of CuPc thin film phototransistor," *Adv. Mater. Res.*, vol. 981, pp. 826–829, Jul. 2014.
[29] P. A. Barrett, C. E. Dent, and R. P. Linstead, "Phthalocyanines. Part VII. Phthalocyanine as a co-ordinating group. A general investigation of the metallic derivatives," *J. Chem. Soc.*, pp. 1719–1736, Sep. 1936.
[30] N. Hayashi, H. Ishii, Y. Ouchi, and K. Seki, "Examination of band bending at buckminsterfullerene (C_{60})/metal interfaces by the Kelvin probe method," *J. Appl. Phys.*, vol. 92, no. 7, pp. 3784–3793, Jul. 2002.
[31] W. Lv *et al.*, "Red light sensitive heterojunction organic field-effect transistors based on neodymium phthalocyanine as photosensitive layer," *Thin Solid Films*, vol. 589, pp. 692–696, Aug. 2015.
[32] Y. Peng *et al.*, "Improved performance of photosensitive field-effect transistors based on palladium phthalocyanine by utilizing Al as source and drain electrodes," *IEEE Trans. Electron Devices*, vol. 60, no. 3, pp. 1208–1212, Mar. 2013.
[33] B. Yao, W. Lv, D. Chen, G. Fan, M. Zhou, and Y. Peng, "Photoresponsivity enhancement of pentacene organic phototransistors by introducing C_{60} buffer layer under source/drain electrodes," *Appl. Phys. Lett.*, vol. 101, no. 16, p. 163301, Oct. 2012.
[34] L. Sun *et al.*, "Ultrahigh near infrared photoresponsive organic field-effect transistors with lead phthalocyanine/C_{60} heterojunction on poly(vinyl alcohol) gate dielectric," *Nanotechnology*, vol. 26, no. 18, p. 185501, Apr. 2015.
[35] J.-P. Xie, W.-I. Lv, T. Yang, B. Yao, and Y.-Q. Peng, "The photoresponsive organic field-effect transistors based on copper phthalocyanine," *Chin. J. Lumimescence*, vol. 33, no. 9, pp. 991–995, Sep. 2012.
[36] J. Xue, S. Uchida, B. P. Rand, and S. R. Forrest, "Asymmetric tandem organic photovoltaic cells with hybrid planar-mixed molecular heterojunctions," *Appl. Phys. Lett.*, vol. 85, no. 23, p. 5757, Dec. 2004.
[37] S. E. Shaheen, R. Radspinner, N. Peyghambarian, and G. E. Jabbour, "Fabrication of bulk heterojunction plastic solar cells by screen printing," *Appl. Phys. Lett.*, vol. 79, no. 18, p. 2996, Oct. 2001.
[38] P. Schilinsky, C. Waldauf, and C. J. Brabec, "Recombination and loss analysis in polythiophene based bulk heterojunction photodetectors," *Appl. Phys. Lett.*, vol. 81, no. 20, p. 3885, Nov. 2002.
[39] F. Yang, M. Shtein, and S. R. Forrest, "Controlled growth of a molecular bulk heterojunction photovoltaic cell," *Nature Mater.*, vol. 4, pp. 37–41, Dec. 2004.
[40] J. Huang and Y. Yang, "Origin of photomultiplication in C_{60} based devices," *Appl. Phys. Lett.*, vol. 91, no. 20, p. 203505, 2007.
[41] Y. Peng *et al.*, "Photo-induced balanced ambipolar charge transport in organic field-effect transistors," *IEEE Photon. Technol. Lett.*, vol. 25, no. 22, pp. 2149–2152, Nov. 15, 2013.
[42] M. Hiramoto, T. Imahigashi, and M. Yokoyama, "Photocurrent multiplication in organic pigment films," *Appl. Phys. Lett.*, vol. 64, no. 2, p. 187, 1994.

Lei Sun is currently pursuing the Ph.D. degree with Lanzhou University, Lanzhou, China.

Yao Li is currently pursuing the Ph.D. degree with Lanzhou University, Lanzhou, China.

Qiang Ren is currently pursuing the master's degree with Lanzhou University, Lanzhou, China.

Wenli Lv is currently pursuing the Ph.D. degree with Lanzhou University, Lanzhou, China.

Jianping Zhang is currently pursuing the master's degree with Lanzhou University, Lanzhou, China.

Xiao Luo is currently pursuing the Ph.D. degree with Lanzhou University, Lanzhou, China.

Feiyu Zhao is currently pursuing the Ph.D. degree with Lanzhou University, Lanzhou, China.

Zhen Chen is currently pursuing the master's degree with China Jiliang University, Hangzhou, China.

Zhanwei Wen is currently pursuing the master's degree with Lanzhou University, Lanzhou, China.

Junkang Zhong is currently pursuing the master's degree with Lanzhou University, Lanzhou, China.

Yingquan Peng received the Ph.D. and Dipl.Ing. degrees from the Humboldt University of Berlin, Berlin, Germany, in 1992.

He is currently a Professor with Lanzhou University, Lanzhou, China.

Xingyuan Liu is currently a Professor with the Changchun Institute of Optics, Fine Mechanics and Physics, Chinese Academy of Sciences, Changchun, China.